Contents lists available at ScienceDirect

Heliyon

Research article

Quantitative proteomics reveals the mechanism of endoplasmic reticulum stress-mediated pulmonary fibrosis in mice

Heng Li [a,b,1], Jin Wang [c,1], Ziling Li [a,b,1], Zhidong Wu [a,b], Yan Zhang [a,b], Lingjia Kong [a,b], Qingqing Yang [a,b], Dong Wang [a,b], He Shi [a,b], Guozheng Shen [a,b], Shuang Zou [a,b], Wenqing Zhu [a,b,***], Kaiyuan Fan [a,b,**], Zhongwei Xu [a,b,*]

[a] Central Laboratory, Logistics University of Chinese People's Armed Police Force, Tianjin, 300309, People's Republic of China
[b] Tianjin key laboratory for prevention and control of occupational and environmental hazards, 300309, People's Republic of China
[c] Department of Clinical Laboratory, Tianjin Third Central Hospital, Tianjin, 300170, People's Republic of China

ARTICLE INFO

ABSTRACT

Pulmonary fibrosis is a progressive disease that can lead to respiratory failure. Many types of cells are involved in the progression of pulmonary fibrosis. This study utilized quantitative proteomics to investigate the mechanism of TGF-β-induced fibrosis-like changes in mouse epithelial cells. Our findings revealed that TGF-β significantly impacted biological processes related to the endoplasmic reticulum, mitochondrion, and ribonucleoprotein complex. Pull-down assay coupled with proteomics identified 114 proteins that may directly interact with TGF-β, and their functions were related to mitochondria, translation, ubiquitin ligase conjugation, mRNA processing, and actin binding. Among them, 17 molecules were also found in different expression proteins (DEPs) of quantitative proteomic, such as H1F0, MED21, SDF2L1, DAD1, and TMX1. Additionally, TGF-β decreased the folded structure and the number of ribosomes in the endoplasmic reticulum and increased the expression of key proteins in the unfolded protein response, including HRD1, PERK, and ERN1. Overall, our study suggested that TGF-β induced fibrotic changes in mouse lung epithelial cells by ER stress and initiated the unfolded protein response through the PRKCSH/IRE1 and PERK/GADD34/CHOP signaling pathways.

1. Introduction

Chronic lung disease can lead to pulmonary fibrosis (PF), characterized by fibroblast proliferation and excessive extracellular matrix (ECM) accumulation in the lung. This condition results in structural abnormalities arising from tissue damage and inflammation [1]. PF-related diseases have complex pathogenesis and are often irreversible. Exogenous stimuli, entering the lungs via the respiratory

---

* Corresponding author. Central Laboratory, Logistics University of Chinese People's Armed Police Force, Tianjin 300309, People's Republic of China. Tianjin key laboratory for preventing and controlling occupational and environmental hazards, 300309, People's Republic of China.

** Corresponding author. Central Laboratory, Logistics University of Chinese People's Armed Police Force, Tianjin, 300309, People's Republic of China.

*** Corresponding author. Central Laboratory, Logistics University of Chinese People's Armed Police Force, Tianjin, 300309, People's Republic of China.

E-mail addresses: 981862381@qq.com (W. Zhu), tcffky1@hotmail.com (K. Fan), xzw113@hotmail.com (Z. Xu).

[1] These authors contributed equally: Heng Li, Jin Wang, and Ziling Li.

tract, activate the innate immune system by acting as non-specific antigens in the alveoli, triggering an early-stage local inflammatory response and promoting the secretion of various cytokines, including IFN-γ, IL-12, and transforming growth factor-β (TGF-β) [2,3]. Typically, the bioactive substances resulting from these exogenous stimuli directly or indirectly stimulate fibroblasts, inducing them to secrete collagen and other ECM components, thus causing irreversible damage to lung tissue and eventually leading to diffuse interstitial fibrosis. Recent studies have explored the cytokine networks' role in mediating inflammation and pulmonary fibrosis, with TGF-β being the most extensively studied cytokine [4]. Macrophages and epithelial cells primarily secrete TGF-β in the lungs, a potent regulator of cell proliferation, stimulating fibroblast proliferation, upregulating procollagen expression, and downregulating collagenase activity, thereby inhibiting collagen degradation [5].

TGF-β is a critical molecule on cell surfaces and within the ECM in pulmonary fibrosis. Numerous studies have demonstrated that exposure to bleomycin (BLM), silica dust, and radiation can induce the onset and progression of pulmonary fibrosis, marked by increased TGF-β expression [6–8]. Its primary function is to activate downstream signaling pathways, notably the classical Smad and non-Smad pathways, which promote epithelial cell proliferation and apoptosis. TGF-β facilitates the differentiation, migration, and invasion of epithelial cells, playing a crucial role in regulating pulmonary fibrosis. TGF-β1 promotes the process of pulmonary fibrosis through various signaling pathways, including Smad, PI3K, MAPK, JNK, p38 and ERK signaling pathways [9]. TGF-β1 induces epithelial-mesenchymal transition (EMT) by activating the NF-κB-YY1 signaling pathway in alveolar epithelial cells [10]. However, several mechanisms and pathways involving TGF-β1 remain unclear. Proteomics can provide a comprehensive and accurate protein quantification strategy to elucidate disease pathogenesis and associated signaling networks. Our results showed that TGF-β treatment induces endoplasmic reticulum stress, which leads to the loss of endoplasmic reticulum (ER) folding morphology and initiation of unfolded protein response (UPR) by PRKCSH/IRE1-mediated ER-associated protein degradation (ERAD) and PERK/GADD34/CHOP signaling pathways.

2. Materials and methods

2.1. Chemicals and reagents

Recombinant mouse TGF-β protein (80116-RNAH) was obtained from Sino Biological (Beijing, China). Fetal bovine serum was from TIANHANG biotechnology (Huzhou, China). Dulbecco's Modified Eagle Medium (DMEM) was from Gibco (NY, USA). Urea (57-13-6) was from Amresco (NZ, USA). Dithiothreitol (R0861), Iodoacetamide (A39271), Protease and Phosphatase Inhibitor Mini Tablets (A32959), The Pierce™ trypsin (90059), TMT-6plex™ Isobaric Label Reagent (90061), Pierce™ NHS-Activated Magnetic Beads (88826), Triethylammonium bicarbonate (90114), Super Signal™ Western (A43840), Pierce Quantitative Peptide Assays Kit (23290) and Pierce BCA Protein Assay Kit (23225) were from Thermo Fisher (Gaithersburg, MD). Anti-Rat IgG (H + L) Cy3 (5230-0361) and DAPI (5930-0006) were from KPL (MD, USA). Radioimmunoprecipitation assay (RIPA) buffer was from Beyotime Biotechnology (Shanghai, China). PRKCSH (12148-1-AP), HRD1(67488-1-Ig), BIP (11587-1-AP), CHOP (15204-1-AP), GADD34 (10449-1-AP), GAPDH (60004-1-Ig) and α-SMA (14395-1-AP) antibodies were from Proteintech (Wuhan, China). PERK(ER64553) and ATF6 (EM1701-94) antibodies were from HuaBio (Hangzhou, China). Sirius red (S8060), 3,3′-diaminobenzidine (D7051), and hematoxylin (H8070) were from Solarbio Life Science (Beijing, China).

2.2. Building the cell and animal model of lung fibrosis

Male C57BL/6 mice (6–8 weeks old, n = 10) were purchased from Beijing Vital River Laboratory Animal Technology (Beijing, China) and housed in accordance with the Guide for the Care and Use of Laboratory Animals. The mice were randomly assigned to 2 groups (n = 5/group): 1) control, 2) BLM). For the pulmonary fibrosis model, mice in BLM group were intratracheally injected with 3 mg/kg BLM, while mice in control group were injected with the same amount of saline for 28 days. Mouse lung epithelial MLE-12 cells were from FengHui Biological Company (Changsha, China), and cells were cultured with H-DMEM containing 10 % FBS at 37 °C. MLE-12 cells were treated with 10 mg/L TGF-β for 0, 12, 24, 36 and 72 h. All the comparisons are against the 0-time point in the subsequent analysis of experimental results.

2.3. Immunofluorescence (ICC) analysis

1×10^4 cells were seeded into the confocal dish cultured for 24 h and treated with 10 mg/L TGF-β. Cells were fixed with 4 % paraformaldehyde for 20 min, permeabilized with 0.5 % Triton X-100 at room temperature for 20 min, and blocked with goat serum. Cells were labeled with rabbit α-SMA, PERK and ATF6 primary antibodies (1:200), and then cells were labeled with anti-Rat IgG (H + L) Cy3(1:1000)and 10 mg/L DAPI. Visualization of fluorescence intensity was captured with a confocal microscope (Leica TCS SP8, Leica).

2.4. Sample preparation for proteomics

After TGF-β treatment, cells were dissolved using lysis buffer containing 8 M urea, 50 mM ammonium bicarbonate and 1 × protease inhibitor, followed by ultrasonic on ice for 5 min. The cell lysate was centrifuged at 4 °C and 13,000 rpm for 10 min, the supernatant was collected and the protein concentration was determined by BCA method. 1 mg of protein in each group was incubated with 1 mM DTT at 60 °C for 30 min and alkylated with 50 mM IAA at room temperature for 30 min. The solution was transferred to an

ultrafiltration device with a 30 kDa cutoff standard and centrifugally enriched at 4 °C and 13,000 rpm for 20 min followed by washed with 50 mM ammonium bicarbonate solution. The protein was digested with 100 μg/mL MS-Grade trypsin at 37 °C for 16h. The digested peptides were desalted using Sep-Pak tC18 Cartridge (Waters, WAT054960), and the concentration was measured using a Quantitative Peptide Assays kit.

The 100 μg peptides in cells treated with 10 mg/L TGF-β at different time intervals were dissolved using 50 μL of 50 mM triethylammonium bicarbonate solution and incubated with ACN solution of TMT-6plex™ Isobaric Label Reagent (126–131) for 1 h followed by quenching the labeling process with 2.5 μL of 5 % NH$_3$OH. The labeled peptides were mixed and desalted using a 1 cc Vac Cartridge of Sep-Pak tC18 and dried using a SpeedVac.

2.5. High-pH RPLC off-line fractionation and nano-LC-MS/MS detection and data analysis

The off-line separation of the mixture labeled peptides was performed according to the previous description [11]. Briefly, the peptides were dissolved using 100 μL 2 % Acetonitrile in H$_2$O (pH = 10) and separated into 20 fractions by Durashell C18 column (5 μm, 250 × 4.6 mm, Agela technologies) using LC3000 (RIGOL Technologies). Each fraction was dissolved in Buffer A (0.1 % formic acid, 98 % H$_2$O, 2 % acetonitrile), loaded onto an EASY-nLC 1000 liquid phase system, captured first by a pre-column (20 mm × 75 μm, A300), and then separated through an analytical column (C18, 200 mm × 75 μm, A200) before entering Q-Exactive HF mass spectrometer (Thermo Fisher Scientific). The nanoLC1000 gradient was 90 min long with a flow rate of 300 nL/min, specifically set as follows: 0–72 min, 5%–21 % Buffer B (0.1 % formic acid, 98 % acetonitrile, 2 % H$_2$O); 72–83 min, 21%–35 % Buffer B; 83–87 min, 35%–99 % Buffer B. The parameters for MS are set as follows: spray voltage of 2.2 kV, MS1 resolution of 60,000, AGC target of 3×10^6, maximum IT of 20 ms, and scan range of 400–1800 m/z. For MS/MS, the resolution is 15,000, the AGC target is 2×10^5, the maximum IT was 100 ms, the collision energy was 35 %, and dynamic exclusion was set to 45 s.

The raw files are analyzed using Proteome Discoverer 2.5 (Thermo Fisher Scientific) with the UniProt *Mus musculus* database selected. The parameters were set as follows: Carbamidomethyl (C) was chosen as the fixed modification, while Oxidation (M), Acetyl (Protein N-term), Met-loss (N-Terminus), Met-loss + Acetyl (M), and TMT-6plex (K) were selected as variable modifications. The integration tolerance was set at 20 ppm, and the False Discovery Rate (FDR) was set to 0.01.

2.6. Pull-down of TGF-β interacting proteins and proteomics analysis

A pull-down assay coupled with proteomics (pull-down proteomics) was performed according to the previous description [12]. According to the instructions, 25 μL of 10 mg/mL NHS-activated magnetic beads and 25 μL of 10 mg/L TGF-β were incubated in an ultra-low binding centrifuge tube at 4 °C for 2 h, with the tube being vortexed every 15 min. The NHS beads and TGF-β complex were placed in a 200 μL of 10 mg/mL valine solution at room temperature for 3 h to block unbound NHS sites followed by washed six times using 0.1M HCl. After incubating the NHS beads and TGF-β complex with 1 mg/mL supernatant of MLE-12 cells for 2 h, TGF-β interaction proteins were collected with an elution buffer with 50 mmol/L Tris-HCl, 5 % β-mercaptoethanol, 2 % SDS and 10 % glycerol. TGF-β-interacting proteins were separated into six fractions by SDS-PAGE based on their molecular weight, which was digestion in GEL with 12.5 μg/mL trypsin followed by analysis using LC-MS/MS according to the previous description [13]. All raw files were uploaded to IPROX (https://www.iprox.cn/) under accession number IPX0008682000.

2.7. Bioinformatics analysis

The differentially expressed proteins (DEPs) were determined based on an absolute Log$_2$ Fold change (FC) value > 0.58 and *P* value < 0.05. DAVID (version 6.8) was used to analyze the Gene Ontology (GO) of DEPs, while Metascape (version 3.5.20240101) and Cytoscape (version 3.7.0) were used for protein interaction analysis. Hiplot was used to analyze gene cluster trends.

2.8. Transmission electron microscope (TEM)

The TEM operation was performed using a previously described method. Briefly, cells were treated with 10 mg/L for 0, 12, 24, 36 and 72 h and fixed with 4 % glutaraldehyde in sodium cacodylate buffer for 2 h. Cells were treated with 1 % osmium tetroxide for 1 h, preserved in paraffin, cut into sections on nickel grids, and stained with 1 % uranyl acetate and 0.5 % lead citrate. The JEOL JEM-1400 EX electron microscope at 100 kV captured morphological images at a magnification of 20,000 × . A diffraction grating replica grid (0.45 μm per square, Ernest Fullam Inc.) was photographed at the same magnification to calibrate.

2.9. Western blot (WB) analysis

Cells were lysed with RIPA buffer, sonicated on ice for 10 min, and centrifuged at 12,000 rpm for 10 min. The supernatant was collected and stored at −80 °C. Protein concentration was determined using a BCA assay (Pierce, Rockford, IL). 30 μg protein samples from each group were then separated by 10 % SDS-PAGE and transferred to nitrocellulose (NC) membranes. The membranes were first incubated with 5 % BSA and incubated overnight at 4 °C with the primary antibodies (diluted at 1:1000) and then incubated for 1 h at room temperature with HRP-labeled secondary antibody (IgG) that was diluted at 1:10,000 (KPL). The intensity was detected with ECL reagent (Millipore, USA) and captured with the Amersham Imager 600 system (GE, UK). The gray values of bands were calculated using ImageJ (version 1.8.0), and GAPDH was used as an internal control.

2.10. Immunohistochemistry (IHC) and sirius red staining analysis

Lung tissues from normal and bleomycin-induced mice were fixed in 4 % paraformaldehyde. The fixed tissues were cut into 5-μm thick sections and embedded in paraffin. After dewaxing and rehydrating, sections were stained with Sirius red reagent. For IHC, the sections are deparaffinized, rehydrated and retrieved antigen sites with citrate buffer according to the previous description [14]. Permeabilization and blocking processes were performed as described above. After labeling with ERN1, HRD1 and PERK antibodies (1:500), the sections were stained with 3,3′-diaminobenzidine and hematoxylin, then photographed under a Nikon DS-Ri2 microscope (Nikon, Japan).

2.11. Statistical analysis

The data were presented as mean ± SD. Statistical analysis was performed using SPSS (version 26.0). ONE-WAY ANOVA was applied to identify significant differences ($P < 0.05$).

3. Results

3.1. TGF-β induced fibrosis of MLE-12

Under microscopic observation, we analyzed the morphological changes in MLE-12 cells after TGF-β treatment. The cells exhibited fibrotic changes at 48 h and an abnormal morphology after 72 h (Fig. 1A). Moreover, we also noted a significant rise in α-SMA protein expression after TGF-β treatment, as detected through ICC analysis (Fig. 1B). These findings implied that TGF-β triggered fibrotic alterations in MLE-12 cells.

3.2. Global quantitative proteomics profiling of TGF-induced MLE-12 cell fibrosis

To investigate the protein changes induced by TGF-β in MLE-12 cells, we collected proteins treated with 10 mg/L TGF-β at different
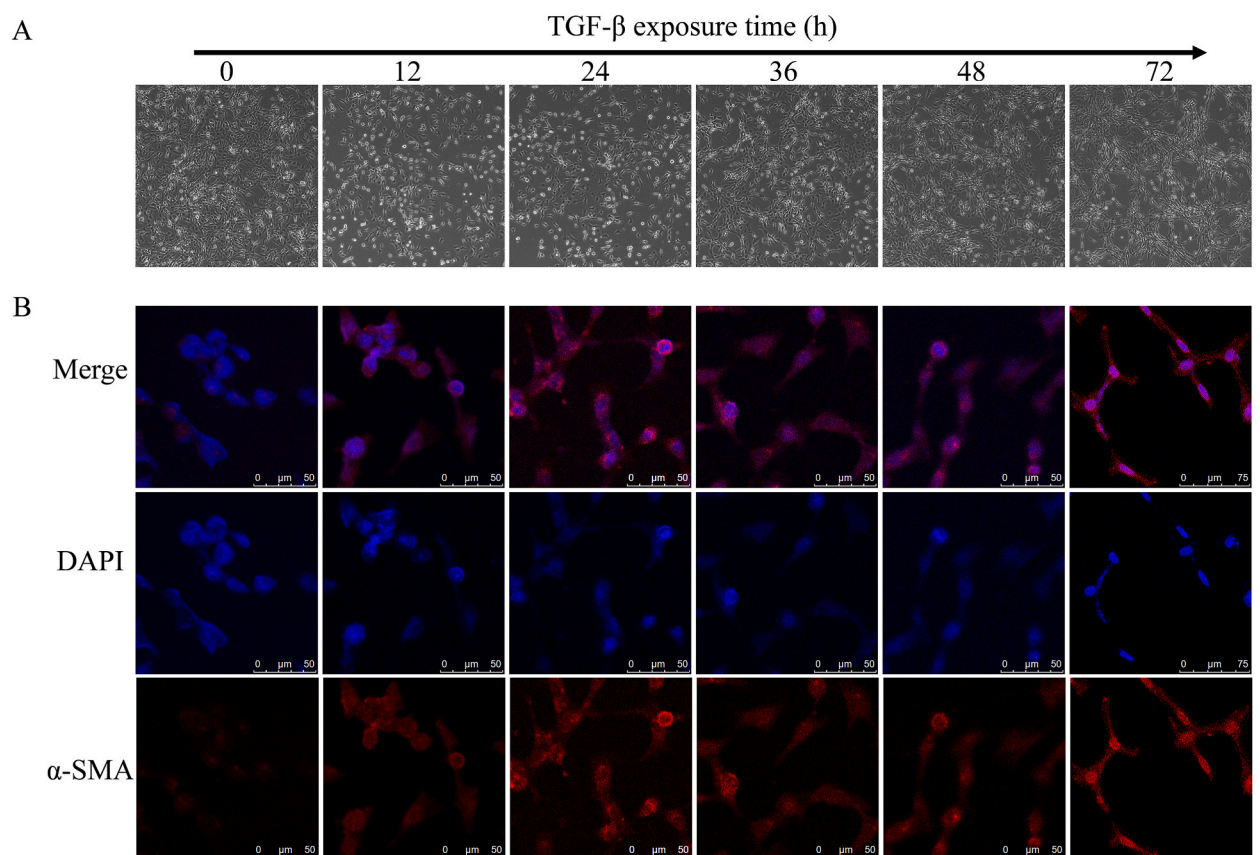
Fig. 1. TGF-β1 induces fibrotic changes in MLE-12 cells. (A) Phase-contrast images of MLE-12 cells in the different groups (0, 12, 24, 36, 48, 72h). Scale bar, 50 μm. (n = 3). (B) Immunofluorescence staining to detect the expression level of α-SMA (red) in MLE-12 cells. Scale bar, 50 μm. (n = 3).

time points and quantitatively identified the proteins using the TMT-6plex labeling method (Fig. 2A). A total of 26,658 peptides corresponding to 6052 proteins were identified, with 783 proteins showing significant changes according to the absolute value of $\log_2$ FC > 0.58 and P value < 0.05. These proteins were classified into four clusters based on their expression patterns (Fig. 2B). Among all experimental groups, the cells treated with TGF-β for 72 h group had the highest number of DEPs, with 491 proteins, including 343 upregulated and 148 downregulated proteins. The DEPs in the 12, 24, 36 and 48 h groups were 298, 379, 153, and 235, respectively (Fig. 2C). 30 proteins showed changes across all 5 experimental groups (Fig. 2D). The principal component analysis (PCA) result showed that the control group was well separated from the other groups. A more distinct separation was observed between the treatment for 72 h and the control group. (Fig. 2D).

3.3. Functional annotation

To study the functions of TGF-β-induced DEPs, functional cluster analysis was performed on these 783 proteins, and Fig. 3A showed the Top 6 with high scores, including endoplasmic reticulum (ER), mitochondrion and ribonucleoprotein complex. We found that upregulated proteins were enriched in the ER and mitochondrion after TGF-β treatment, including IRE1, CANX, SEC61, MTCH2, TFRC, and TUSC3. In contrast, downregulated proteins were mostly enriched in isopeptide bond and RNA binding, including EEF1B2, RPS15, SRRM1, SRSF2, IMPDH2, and EIF3G (Fig. 3B).

In the pull-down proteomics analysis, 114 proteins interacting with TGF-β were identified, of which 17 were also detected in the quantitative proteomics analysis of the treated group (Fig. 3C). These proteins were enriched in ER and cytosol (Fig. 3D). Together, these results suggest that the ER function of MLE-12 might be altered after TGF-β treatment. We screened for ER-associated proteins to conduct a specific functional analysis and found that 13 DEPs were involved in COPII-mediated vesicle transport, 12 DEPs were involved in Integration of energy metabolism, and 11 DEPs were involved in Protein folding (Fig. 3E).

3.4. TEM analysis of ER

Fig. 4A showed the morphology of the ER under TEM, aiming to establish a relationship between TGF-β-induced MLE-12 fibrosis and ER. Compared to the control group, the morphology of the ER changed over time following TGF-β treatment, primarily manifested as the loss of the normal folded structure and a decrease in the number of ribosomes associated with the ER. Meanwhile, the morphological changes of the ER were more significant when the treatment time reached 48 h. Additionally, the morphological changes of the ER were more pronounced at 48 h of treatment. These results suggest that TGF-β-induced fibrosis in MLE-12 cells is closely associated with alterations in the ER.

3.5. Validation of the proteomics results for ER-stress in vitro

Many ER-related proteins, including PERK, ATF6, BIP, CHOP, PRKCSH, HRD1 and GADD34, were further validated using WB and
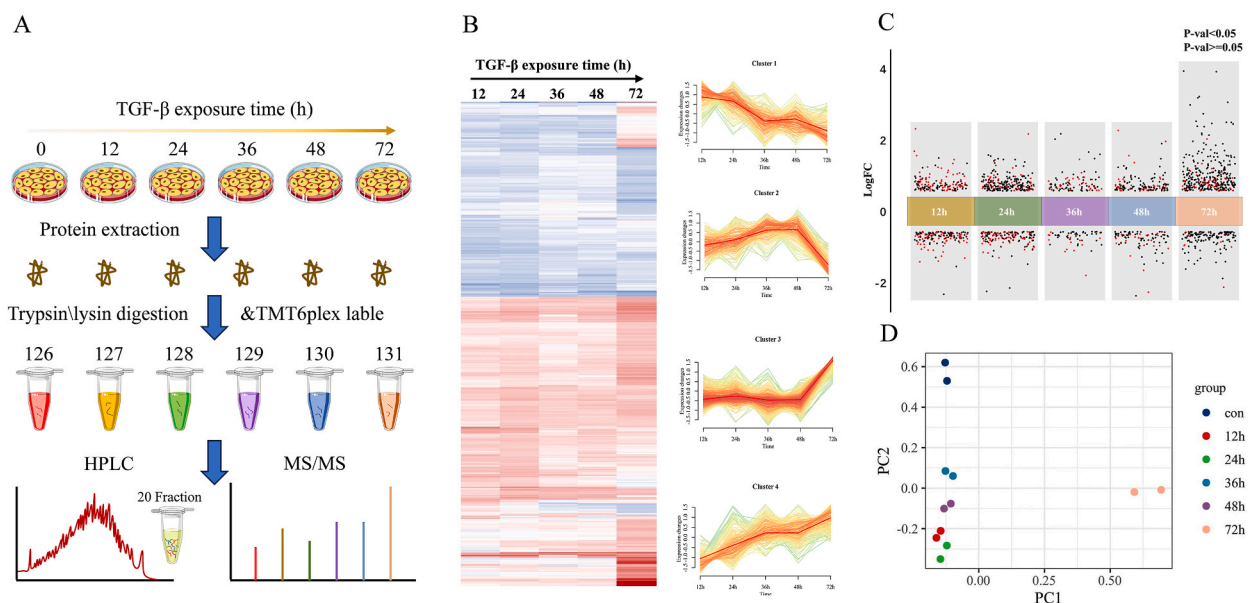
Fig. 2. Proteomic profiling of TGF-β1 treated MLE-12 cells. (A) Workflow was used in this study. (B) Hierarchical clustering analysis (showing on left) and gene cluster trend (showing on right) of all 783 DEPs. (C) Volcano plot of filtered DEPs(red). Filtering criteria were an absolute value of $\log_2$ FC > 0.58 and P value < 0.05. (D) Principal component analysis results of different groups (0, 12, 24, 36, 48, 72h) using quantified proteins.
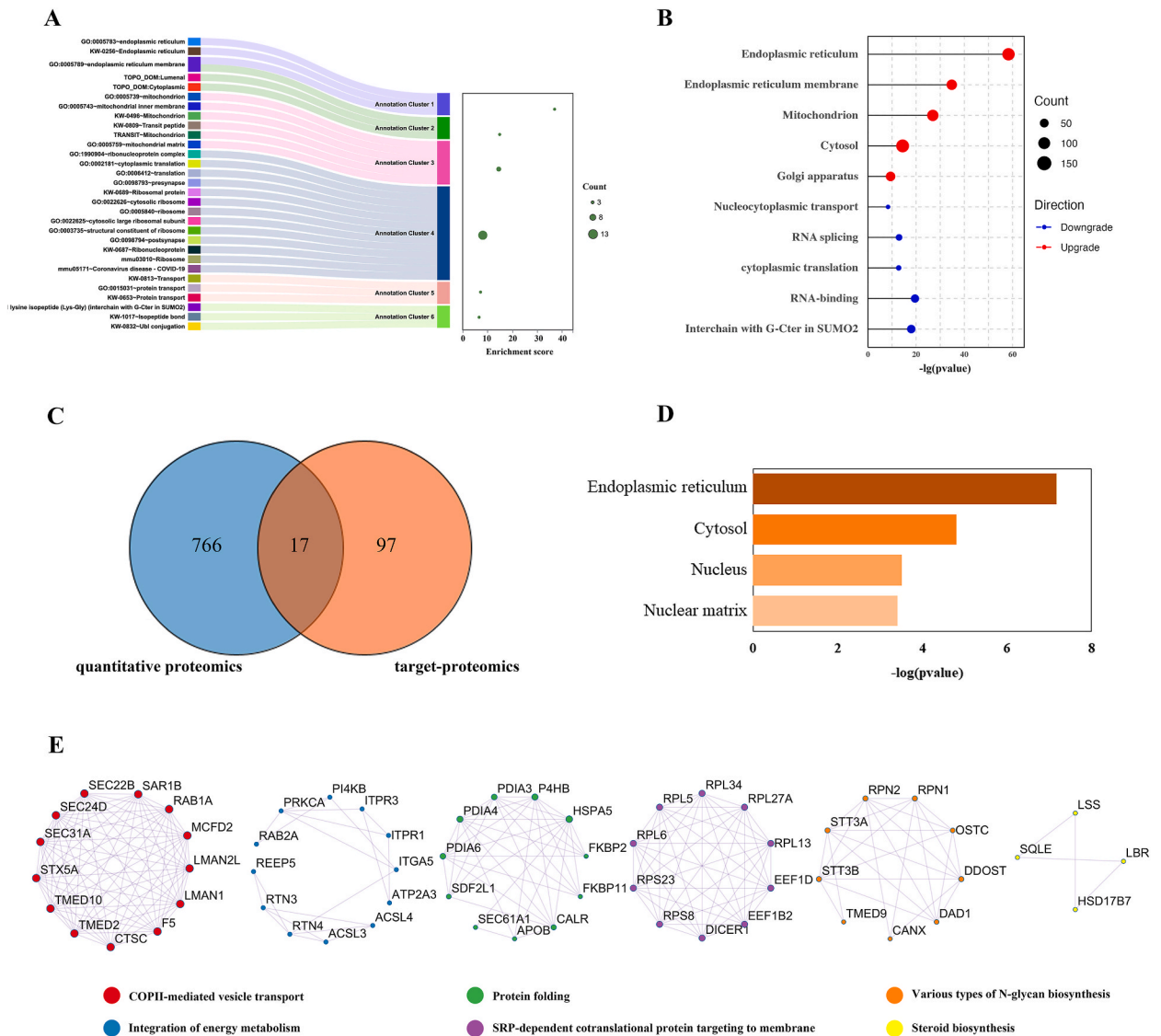
Fig. 3. Functional annotation cluster and GO analysis of DEPs. (A) TOP 6 functional annotation clusters of all 783 DEPs. (B) TOP 5 functional annotation classifications of up (red) or down (down) regulated proteins in all six groups. (C) Venn analysis showing the number of proteins identified in quantitative proteomics and pull-down proteomics. (D) Biological processes analysis of the 17 proteins shared between quantitative proteomics and pull-down proteomics. (E) Protein–protein interaction network of DEPs, which are involved in ER-related process.

ICC (Fig. 4B–C). The results showed that the expression of PRKCSH protein increased after TGF-β treatment ($P < 0.05$). Compared to the control group, the expression levels of PERK and CHOP in TGF-β treatment were significantly increased at 24 h ($P < 0.05$) and significantly decreased at 72 h ($P < 0.05$). The expression level of GADD34 trended upward and reached the maximum at 48 h ($P < 0.05$), while the ATF6 expression level showed a decreased trend and reached the minimum at 72 h ($P < 0.05$). The HRD1 expression level was significantly increased at 12, 24 and 36 h ($P < 0.05$). The BIP expression level was significantly decreased at 72 h ($P < 0.05$). ICC results showed that the fluorescence intensity of ATF6 gradually decreased, and the fluorescence intensity of PERK increased first and then decreased, which was consistent with the WB results.

3.6. The results of bleomycin-induced fibrosis using sirius red staining and WB in vivo

Some lung cells in the bleomycin treatment group were stained and appeared brownish-yellow compared to the control group, suggesting the occurrence of myocyte fibrosis (Fig. 5A). Compared with the control group, the expression level of HRD1 was significantly increased in the bleomycin treatment group, while the expression level of ATF6 was significantly decreased (P < 0.05) (Fig. 5B–C).
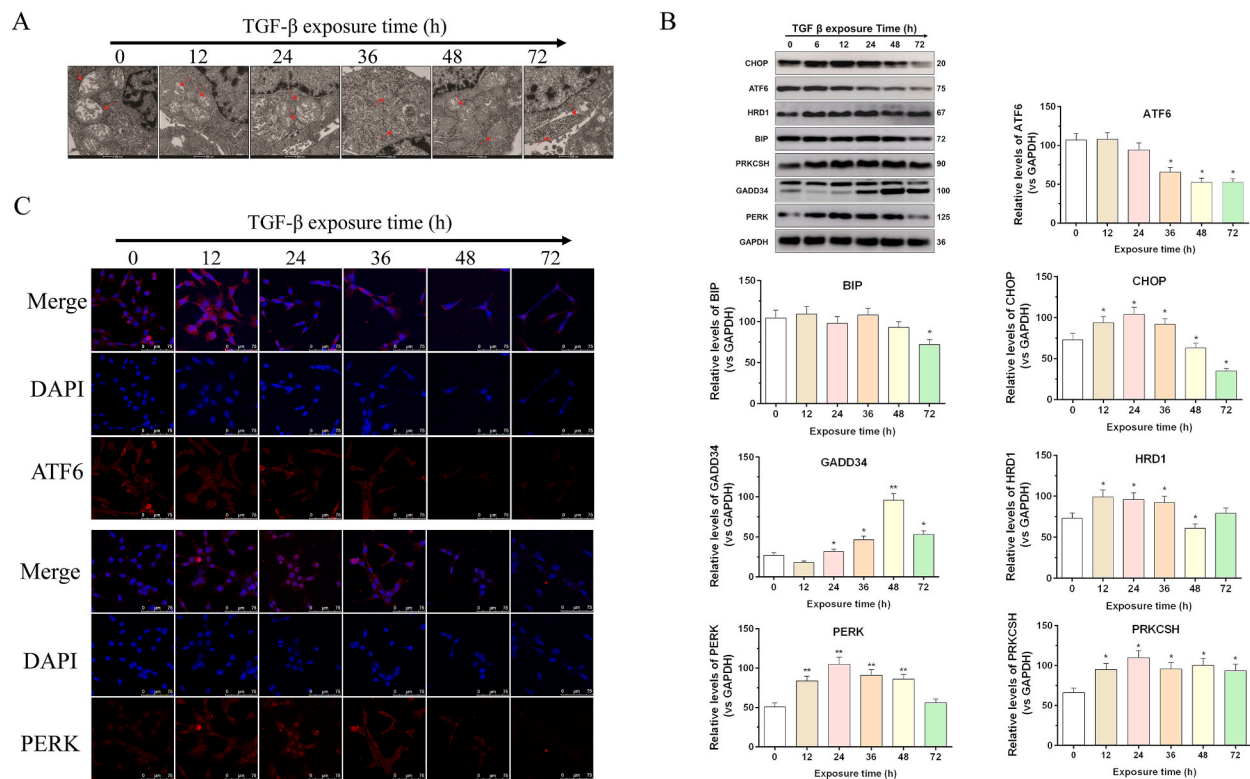
Fig. 4. TGF-β-induced ER-stress in MLE-12. (A) Transmission electron microscopy analysis showing ER morphology (arrowed). (B) Western blot analysis of PERK, ATF6, BIP, CHOP, PRKCSH, HRD1, GADD34 (Supplementary information, Figs. S2–S9). Histograms display the densitometry measurements of bands, with GAPDH levels serving as the reference control (n = 3 per group). (D) Immunofluorescence staining to detect expression levels of ATF6 (red) and PERK (red). Scale bar, 75 μm. (n = 3).

3.7. Mechanism of TGF-β-induced ER-stress

Combined with the results of MS and WB, we presented the DEPs related to the structure and function of the ER in the signaling pathway (Fig. 6). SEC61 and SEC63 work together to transport polypeptides to the ER via translocation. PRKCSH, PDIA3, CALR, and CANX are involved in protein folding. SAR1B, SEC24, and LMAN1 play a vital role in transporting properly folded proteins to the extracellular layer. PDIA4, ERP29, and SSR3 could target misfolded proteins to the ER or cytoplasm for ubiquitination degradation (UBE2G2, SE1LE, HRD1), and the accumulation of misfolded proteins induces ER stress (PERK, ATF6, IRE1). STT3A, STT3B, DAD1, and TUSC3 are responsible for glycosylation modification of ER proteins. Among these DEPs, most of them showed an increasing trend, indicating the occurrence of ER stress, especially for the N-Glycan biosynthesis and ERAD.

4. Discussion

Alveoli are encased by a single layer of epithelial cells, wherein alveolar epithelial type 1 (AT1) and type 2 (AT2) cells serve as the primary sites for gas exchange. Fibroblast proliferation in the subepithelial interstitial area and ECM deposition typify pulmonary fibrosis [15]. Although fibroblasts are primarily responsible for ECM production in fibrosis, alveolar epithelial cells also play a crucial role; notably, damage to these cells is a key driver of fibrosis [16,17]. AT1 cells have reached their terminal developmental stage, whereas AT2 cells produce surfactant and have the potential to differentiate into AT1 cells. Senescence in AT2 cells impairs their differentiation capacity and surfactant secretion, culminating in the failure of epithelial repair [18,19]. TGF-β overexpression in mice initially reduces surfactant proteins B (SP-B) and SP-C before lung fibrosis [20]. AT2 cells may transform into fibroblasts or activate them through cytokine release [21]. Our study demonstrated that TGF-β can induce endoplasmic reticulum stress, leading to fibrosis-like changes in mouse AT2 MLE-12 cells.

Combining quantitative and pull-down proteomics results, we find that TGF-β-induced MLE-12 cell fibrosis involves various cellular processes, including ER and mitochondrial stress, translation, Golgi apparatus function, RNA splicing, and ER to Golgi vesicle-mediated transport. Pull-down proteomics identifies 114 proteins potentially interacting directly with TGF-β, with functions related to mitochondrial operations, translation, ubiquitin ligase conjugation, mRNA processing, and actin binding. Among them, 17 of these proteins are also found in DEPs of quantitative proteomics, including ACTB, H1F0, MED21, GTF2A1, ACOT13, SDF2L1, RBPMS, MTPN, DAD1, TMX1, SGPL1, ERH, ATXN10, PRDX2, PGRMC2, S100A10, and ARG10. Studies show that the level of ACTB in the
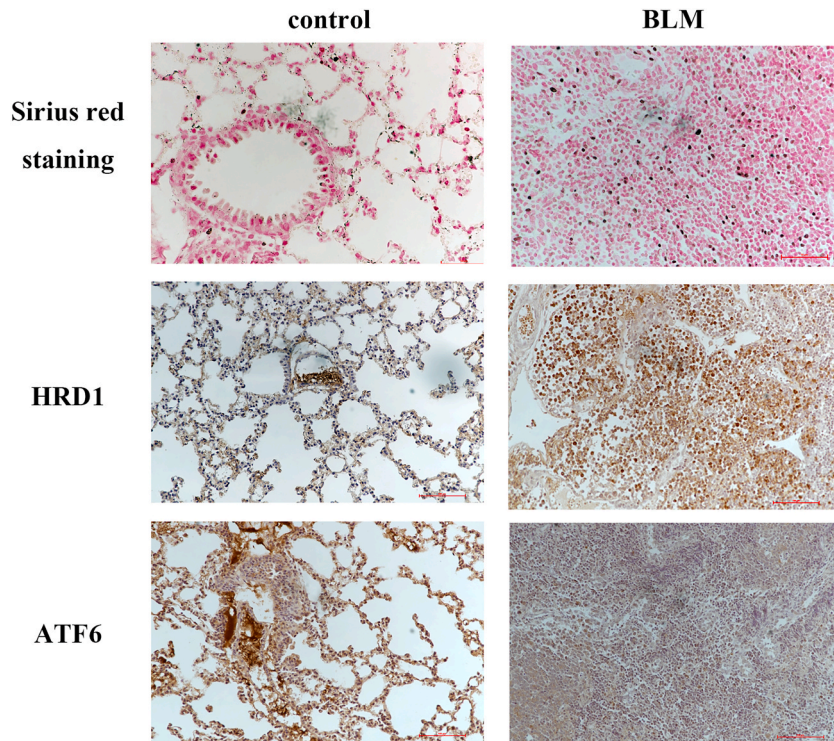
Fig. 5. Bleomycin-induced fibrosis of mouse lung tissues. (A) Sirius red-stained images of mouse lung tissues. The expression level of ATF6 (B) and (C) of lung tissue. Scale bar, 100 μm. (n = 3).
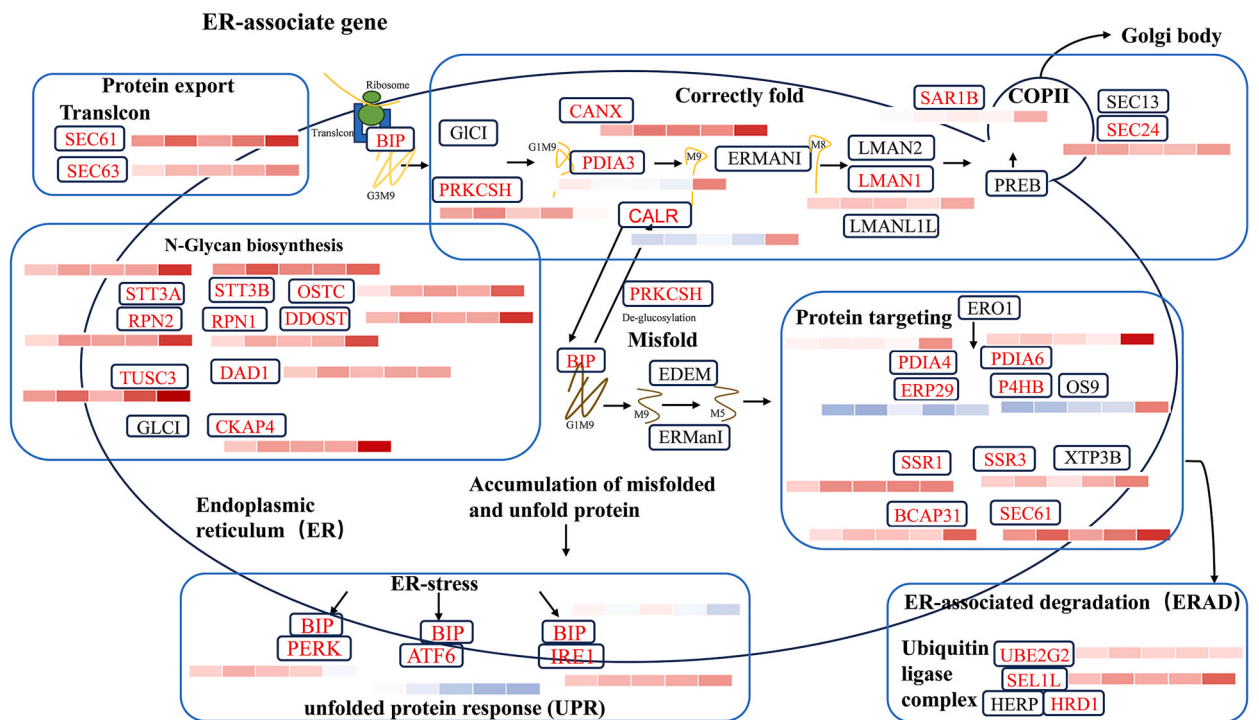

Fig. 6. The potential mechanism of TGF-β-induced ER-stress.

alveolar lavage fluid increases in patients with severe pulmonary interstitial disease. Treatment with ACTB enhances α-SMA and collagen I gene expression in fibroblasts [22]. The localization of SDF2L1 to the ER could activate the entry of misfolded proteins into the ERAD pathway by forming polyprotein complexes with BIP [23]. ERH, a highly conserved protein that interacts with EIF2α, and regulates the EIF2α-ATF4/CHOP signaling pathway to induce ER stress [24]. TMX1, an important thioredoxin in the mitochondria-associated membranes, transforms ER stress caused by protein accumulation [25]. In conclusion, pull-down proteomics provides clues to the association between TGF-β induced pulmonary fibrosis mechanisms and ER stress.

The ER is a critical cellular structure for protein processing, transportation, folding, and modification of glycosylation. Dysfunction of the ER has been linked to various fibrotic diseases such as kidney, lung, and liver diseases [26–28]. Our bioinformatics analysis indicated that TGF-β treatment is closely associated with ER function by impacting the protein transport, folding, and N-glycan biosynthesis in MLE-12 cells. Studies show that mutations or accumulation in the BRICHOS domain of the SP-C protein induce ER stress, thereby triggering apoptosis in endothelial cells [29]. The PERK, ATF6, and IRE1 proteins can activate the UPR process under ER stress, serving as a crucial defense mechanism to restore proper protein folding and cellular homeostasis [30]. After treatment with TGF-β, the expression of PRKCSH, IRE1 and PERK levels in MLE-12 cells show an increasing trend. PRKCSH, a selective activator of IRE1, promotes the autophosphorylation and oligomerization of IRE1α [31]. IRE1 cleaves the transcription factor XBP1 upon activation, which is subsequently translocated to the nucleus to initiate the ERAD process [32]. Once activated, PERK reduces protein translation by recruiting and phosphorylating the translation initiation factor eIF2α [33]. Our findings indicate an increase in the expression of UBE2G2, SEL1L, and HRD1, which are related to ERAD and involved in ubiquitination function. UBE2G2 is classified as an E2 ubiquitin-conjugating enzyme, while HRD1 is categorized as an E3 ubiquitin-ligase enzyme. The proper functioning of HRD1, which includes responsible protein stability, substrate recruitment, and ubiquitination, is contingent upon its interaction with SEL1L [34–36]. Study shows that overexpression of HRD1 increased collagen secretion in renal epithelial cells, resulting in aggravated renal fibrosis in mice [37]. Additionally, we also find that the downstream PERK molecules GADD34 and CHOP expression levels increased in the TGF-β treatment. CHOP-mediated GADD34 can restore protein synthesis through eIF2α dephosphorylation, accumulating unfolded proteins in the endoplasmic reticulum and leading to apoptosis [38]. Many studies demonstrate that activation of GADD34 and CHOP reduces myofibroblasts' migration and proliferation capacities in rat liver fibrosis but promotes angiogenic activity [39].

In this study, we initially observe fibrosis-like changes in MLE-12 cells following exposure to TGF-β. Employing proteomics and bioinformatics analysis, we determine that the DEPs were closely associated with ER function. Subsequently, we note a reduction in the folded morphology of the ER and an increase in the expression of hallmark ER stress proteins, PERK and IRE1. ER stress has been demonstrated to induce dysfunction in AT2 cells, leading to fibrosis [40]. Engeletin can ameliorate TGF-β-stimulated pulmonary fibrosis through endoplasmic reticulum stress [41]. Thus, our results suggest that TGF-β induces fibrotic changes in mouse lung epithelial cells through ER stress and initiates the UPR via PRKCSH/IRE1 and PERK/GADD34/CHOP signaling pathways. In future studies, animal experiments combined with glycosylation and ubiquitination proteomics are expected to elucidate the mechanisms underlying pulmonary fibrosis more precisely.

CRediT authorship contribution statement

Heng Li: Writing – original draft, Methodology, Data curation. **Jin Wang:** Writing – review & editing. **Ziling Li:** Methodology, Data curation. **Zhidong Wu:** Supervision, Conceptualization. **Yan Zhang:** Formal analysis, Supervision. **Lingjia Kong:** Data curation. **Qingqing Yang:** Data curation. **Dong Wang:** Data curation. **He Shi:** Data curation. **Guozheng Shen:** Data curation. **Shuang Zou:** Data curation. **Wenqing Zhu:** Validation, Conceptualization, Methodology. **Kaiyuan Fan:** Software, Validation, Data curation. **Zhongwei Xu:** Funding acquisition, Writing – review & editing, Formal analysis.

Ethics statement

The study was conducted according to the Guide for the Care and Use of Laboratory Animals and approved by the Institutional Animal Care and Use Committee of Logistics University of Chinese People's Armed Police Force (Approval No. 20230020).

Data availability statement

The datasets presented in this study can be found in online repositories. The names of the repository/repositories and accession number(s) can be found in the article.

Funding

Declaration of competing interest

The authors declare that they have no known competing financial interests or personal relationships that could have appeared to influence the work reported in this paper.

Appendix A. Supplementary data

Supplementary data to this article can be found online at https://doi.org/10.1016/j.heliyon.2024.e39150.

References

[1] T. Koudstaal, M. Funke-Chambour, M. Kreuter, P.L. Molyneaux, M.S. Wijsenbeek, Pulmonary fibrosis: from pathogenesis to clinical decision-making, Trends Mol. Med. (2023), https://doi.org/10.1016/j.molmed.2023.08.010.
[2] N. Singh, N. Arora, Diesel exhaust exposure in mice induces pulmonary fibrosis by TGF-β/Smad3 signaling pathway, Sci. Total Environ. 807 (2022) 150623, https://doi.org/10.1016/j.scitotenv.2021.150623.
[3] S. Xiong, R. Guo, Z. Yang, L. Xu, L. Du, R. Li, F. Xiao, Q. Wang, M. Zhu, X. Pan, Treg depletion attenuates irradiation-induced pulmonary fibrosis by reducing fibrocyte accumulation, inducing Th17 response, and shifting IFN-γ, IL-12/IL-4, IL-5 balance, Immunobiology 220 (11) (2015) 1284–1291, https://doi.org/10.1016/j.imbio.2015.07.001.
[4] N. Inui, S. Sakai, M. Kitagawa, Molecular pathogenesis of pulmonary fibrosis, with focus on pathways related to TGF-β and the ubiquitin-proteasome pathway, Int. J. Mol. Sci. 22 (11) (2021) 6107, https://doi.org/10.3390/ijms22116107.
[5] A. Saito, M. Horie, T. Nagase, TGF-β signaling in lung health and disease, Int. J. Mol. Sci. 19 (8) (2018) 2460, https://doi.org/10.3390/ijms19082460.
[6] K.R. Cutroneo, S.L. White, S.H. Phan, H.P. Ehrlich, Therapies for bleomycin induced lung fibrosis through regulation of TGF-β1 induced collagen gene expression, J. Cell. Physiol. 211 (3) (2007) 585–589, https://doi.org/10.1002/jcp.20972.
[7] Z.-q. Zhang, H.-t. Tian, H. Liu, R. Xie, The role of macrophage-derived TGF-β1 on SiO2-induced pulmonary fibrosis: a review, Toxicol. Ind. Health 37 (4) (2021) 240–250, https://doi.org/10.1177/0748233721989896.
[8] M. Yi, Y. Yuan, L. Ma, L. Li, W. Qin, B. Wu, B. Zheng, X. Liao, G. Hu, B. Liu, Inhibition of TGFβ1 activation prevents radiation-induced lung fibrosis, Clin. Transl. Med. 14 (1) (2024) e1546, https://doi.org/10.1002/ctm2.1546.
[9] Z. Ye, Y. Hu, TGF-β1: gentlemanly orchestrator in idiopathic pulmonary fibrosis, Int. J. Mol. Med. 48 (1) (2021) 1–14, https://doi.org/10.3892/ijmm.2021.4965.
[10] C. Zhang, X. Zhu, Y. Hua, Q. Zhao, K. Wang, L. Zhen, G. Wang, J. Lü, A. Luo, W.C. Cho, YY1 mediates TGF-β1-induced EMT and pro-fibrogenesis in alveolar epithelial cells, Respir. Res. 20 (2019) 1–11, https://doi.org/10.1186/s12931-019-1223-7.
[11] Z. Xu, J. Bao, X. Jin, H. Li, K. Fan, Z. Wu, M. Yao, Y. Zhang, G. Liu, D. Wang, The effects of cinobufagin on hepatocellular carcinoma cells enhanced by MRT68921, an autophagy inhibitor, Am. J. Chin. Med. 51 (6) (2023) 1595–1611, https://doi.org/10.1142/S0192415X23500726.
[12] H. Vais, M. Wang, K. Mallilankaraman, R. Payne, C. Mckennan, J.T. Lock, L.A. Spruce, C. Fiest, Y.L. Chan, I. Parker, ER-luminal [Ca2+] regulation of InsP3 receptor gating mediated by an ER-luminal peripheral Ca2+-binding protein, Elife 9 (2020), https://doi.org/10.7554/eLife.53531.
[13] D. Botelho, M.J. Wall, D.B. Vieira, S. Fitzsimmons, F. Liu, A. Doucette, Top-down and bottom-up proteomics of SDS-containing solutions following mass-based separation, J. Proteome Res. 9 (6) (2010) 2863–2870, https://doi.org/10.1021/pr900949p.
[14] T. Yao, H. Hou, G. Liu, J. Wu, Z. Qin, Y. Sun, X. Jin, J. Chen, Y. Chen, Z. Xu, Quantitative proteomics suggest a potential link between early embryonic death and trisomy 16, Reprod. Fertil. Dev. 31 (6) (2019) 1116–1126, https://doi.org/10.1071/RD17319.
[15] A. Pardo, M. Selman, Molecular mechanisms of pulmonary fibrosis, Front. Biosci. 7 (1) (2002) 1743–1761, https://doi.org/10.2741/pardo.
[16] I.A. Savin, M.A. Zenkova, A.V. Sen'kova, Pulmonary fibrosis as a result of acute lung inflammation: molecular mechanisms, relevant in vivo models, prognostic and therapeutic approaches, Int. J. Mol. Sci. 23 (23) (2022) 14959, https://doi.org/10.3390/ijms232314959.
[17] P.W. Noble, C.E. Barkauskas, D. Jiang, Pulmonary fibrosis: patterns and perpetrators, J. Clin. Invest. 122 (8) (2012) 2756–2762, https://doi.org/10.1172/JCI60323.
[18] S. Sitaraman, K.-D. Alysandratos, J.A. Wambach, M.P. Limberis, Gene therapeutics for surfactant dysfunction disorders: targeting the alveolar type 2 epithelial cell, Hum, Gene Ther. 33 (19–20) (2022) 1011–1022, https://doi.org/10.1089/hum.2022.130.
[19] P. Confalonieri, M.C. Volpe, J. Jacob, S. Maiocchi, F. Salton, B. Ruaro, M. Confalonieri, L. Braga, Regeneration or repair? The role of alveolar epithelial cells in the pathogenesis of idiopathic pulmonary fibrosis (IPF), Cells 11 (13) (2022) 2095, https://doi.org/10.3390/cells11132095.
[20] E. Lopez-Rodriguez, C. Boden, M. Echaide, J. Perez-Gil, M. Kolb, J. Gauldie, U.A. Maus, M. Ochs, L. Knudsen, Surfactant dysfunction during overexpression of TGF-β1 precedes profibrotic lung remodeling in vivo, Am. J. Physiol. Lung Cell Mol. Physiol. 310 (11) (2016) L1260–L1271, https://doi.org/10.1152/ajplung.00065.2016.
[21] L. Yao, Y. Zhou, J. Li, L. Wickens, F. Conforti, A. Rattu, F.M. Ibrahim, A. Alzetani, B.G. Marshall, S.V. Fletcher, Bidirectional epithelial–mesenchymal crosstalk provides self-sustaining profibrotic signals in pulmonary fibrosis, J. Biol. Chem. 297 (3) (2021), https://doi.org/10.1016/j.jbc.2021.101096.
[22] G. Cooke, P. Govender, C. Watson, M. Armstrong, D. O'Dwyer, M. Keane, R. King, A. Tynan, M. Dunn, S. Donnelly, Sarcoidosis, alveolar β-actin and pulmonary fibrosis, QJM: Int. J. Med. 106 (10) (2013) 897–902, https://doi.org/10.1093/qjmed/hct160.
[23] T. Sasako, M. Ohsugi, N. Kubota, S. Itoh, Y. Okazaki, A. Terai, T. Kubota, S. Yamashita, K. Nakatsukasa, T. Kamura, Hepatic Sdf2l1 controls feeding-induced ER stress and regulates metabolism, Nat. Commun. 10 (1) (2019) 947, https://doi.org/10.1038/s41467-019-08591-6.
[24] K. Pang, Y. Dong, L. Hao, Z.-d. Shi, Z.-g. Zhang, B. Chen, H. Feng, Y.-y. Ma, H. Xu, D. Pan, ERH interacts with EIF2α and regulates the EIF2α/ATF4/CHOP pathway in bladder cancer cells, Front. Oncol. 12 (2022) 871687, https://doi.org/10.3389/fonc.2022.871687.
[25] Y. Matsuo, Y. Nishinaka, S. Suzuki, M. Kojima, S. Kizaka-Kondoh, N. Kondo, A. Son, J. Sakakura-Nishiyama, Y. Yamaguchi, H. Masutani, TMX, a human transmembrane oxidoreductase of the thioredoxin family: the possible role in disulfide-linked protein folding in the endoplasmic reticulum, Arch. Biochem. Biophys. 423 (1) (2004) 81–87, https://doi.org/10.1016/j.abb.2003.11.003.
[26] A.V. Cybulsky, Endoplasmic reticulum stress, the unfolded protein response and autophagy in kidney diseases, Nat. Rev. Nephrol. 13 (11) (2017) 681–696, https://doi.org/10.1038/nrneph.2017.129.
[27] E. Martínez-Klimova, O.E. Aparicio-Trejo, T. Gómez-Sierra, A.P. Jiménez-Uribe, B. Bellido, J. Pedraza-Chaverri, Mitochondrial dysfunction and endoplasmic reticulum stress in the promotion of fibrosis in obstructive nephropathy induced by unilateral ureteral obstruction, Biofactors 46 (5) (2020) 716–733, https://doi.org/10.1002/biof.1673.
[28] M. Bueno, M. Rojas, Lost in translation: endoplasmic reticulum–mitochondria crosstalk in idiopathic pulmonary fibrosis, Am. J. Respir. Cell Mol. Biol. 63 (4) (2020) 408–409, https://doi.org/10.1165/rcmb.2020-0273ED.
[29] S. Mulugeta, V. Nguyen, S.J. Russo, M. Muniswamy, M.F. Beers, A surfactant protein C precursor protein BRICHOS domain mutation causes endoplasmic reticulum stress, proteasome dysfunction, and caspase 3 activation, Am. J. Respir. Cell Mol. Biol. 32 (6) (2005) 521–530, https://doi.org/10.1165/rcmb.2005-0009OC.
[30] S.A. Oakes, F.R. Papa, The role of endoplasmic reticulum stress in human pathology, Annu. Rev. Pathol.: Mech. Dis. 10 (2015) 173–194, https://doi.org/10.1146/annurev-pathol-012513-104649.
[31] G.-C. Shin, S.U. Moon, H.S. Kang, H.-S. Choi, H.D. Han, K.-H. Kim, PRKCSH contributes to tumorigenesis by selective boosting of IRE1 signaling pathway, Nat. Commun. 10 (1) (2019) 3185, https://doi.org/10.1038/s41467-019-11019-w.
[32] S.-M. Park, T.-I. Kang, J.-S. So, Roles of XBP1s in transcriptional regulation of target genes, Biomedicines 9 (7) (2021) 791, https://doi.org/10.3390/biomedicines9070791.
[33] A. McQuiston, J.A. Diehl, Recent insights into PERK-dependent signaling from the stressed endoplasmic reticulum, F1000Research 6 (2017), https://doi.org/10.12688/f1000research.12138.1.

[34] K.S. Chakrabarti, J. Li, R. Das, R.A. Byrd, Conformational dynamics and allostery in E2: E3 interactions drive ubiquitination: gp78 and Ube2g2, Structure 25 (5) (2017) 794–805. e5, https://doi.org/10.1016/j.str.2017.03.016.

[35] N. Shrestha, T. Liu, Y. Ji, R.B. Reinert, M. Torres, X. Li, M. Zhang, C.-H.A. Tang, C.-C.A. Hu, C. Liu, Sel1L-Hrd1 ER-associated degradation maintains β cell identity via TGF-β signaling, J. Clin. Invest. 130 (7) (2020) 3499–3510, https://doi.org/10.1172/JCI134874.

[36] L.L. Lin, H.H. Wang, B. Pederson, X. Wei, M. Torres, Y. Lu, Z.J. Li, X. Liu, H. Mao, H. Wang, SEL1L-HRD1 interaction is required to form a functional HRD1 ERAD complex, Nat. Commun. 15 (1) (2024) 1440, https://doi.org/10.1038/s41467-024-45633-0.

[37] L. Li, Y. Shen, Y. Ding, Y. Liu, D. Su, X. Liang, Hrd1 participates in the regulation of collagen I synthesis in renal fibrosis, Mol. Cell. Biochem. 386 (2014) 35–44, https://doi.org/10.1007/s11010-013-1843-z.

[38] S.J. Marciniak, C.Y. Yun, S. Oyadomari, I. Novoa, Y. Zhang, R. Jungreis, K. Nagata, H.P. Harding, D. Ron, CHOP induces death by promoting protein synthesis and oxidation in the stressed endoplasmic reticulum, Genes Dev. 18 (24) (2004) 3066–3077, https://doi.org/10.1101/gad.1250704.

[39] E. Loeuillard, H. El Mourabit, L. Lei, S. Lemoinne, C. Housset, A. Cadoret, Endoplasmic reticulum stress induces inverse regulations of major functions in portal myofibroblasts during liver fibrosis progression, Biochim. Biophys. Acta, Mol. Basis Dis. 1864 (12) (2018) 3688–3696, https://doi.org/10.1016/j.bbadis.2018.10.008.

[40] Z. Borok, M. Horie, P. Flodby, H. Wang, Y. Liu, S. Ganesh, A.L. Firth, P. Minoo, C. Li, M.F. Beers, Grp78 loss in epithelial progenitors reveals an age-linked role for endoplasmic reticulum stress in pulmonary fibrosis, Am. J. Respir. Crit. Care Med. 201 (2) (2020) 198–211, https://doi.org/10.1164/rccm.201902-0451OC.

[41] Z. Jinjin, C. Xiaoqing, C. Hongbin, L. Rongrong, X. Pan, L. Changjun, Engeletin ameliorates pulmonary fibrosis through endoplasmic reticulum stress depending on lnc949-mediated TGF-β1-Smad2/3 and JNK signalling pathways, Pharm. Biol. 58 (1) (2020) 1114–1123, https://doi.org/10.1080/13880209.2020.1834590.